# Ultra-broadband fiber filter based on chirped highly localized fiber Bragg gratings

Yu Fan,<sup>1,2</sup> Weijia Bao,<sup>1,2,\*</sup> Jiajun Guan,<sup>1,2</sup> CHANGRUI LIAO, 1,2 D AND YIPING WANG 1,2 D

<sup>1</sup>Shenzhen Key Laboratory of Photonic Devices and Sensing Systems for Internet of Things, Guangdong and Hong Kong Joint Research Centre for Optical Fibre Sensors, State Key Laboratory of Radio Frequency Heterogeneous Integration, Shenzhen University, Shenzhen 518060, China <sup>2</sup>Shenzhen Key Laboratory of Ultrafast Laser Micro/Nano Manufacturing, Key Laboratory of Optoelectronic Devices and Systems of Ministry of Education/Guangdong Province, College of Physics and Optoelectronic Engineering, Shenzhen University, Shenzhen 518060, China wjbao@szu.edu.cn

**Abstract:** Broadband optical filters are highly useful tools in many fields, such as supercontinuum light sources, astronomical observations, and optical coherence tomography. However, conventional broadband filters have limited bandwidth and relatively high insertion loss (IL). In this study, an ultra-broadband fiber filter based on a chirped highly localized fiber Bragg grating (CHLFBG) is fabricated via a femtosecond laser point-by-point inscription technique, which is demonstrated for the first time to the best of our knowledge. This filter provides optical suppression exceeding 90% (-10 dB) over a bandwidth of larger than 500 nm, which extends across the O + E + S + C + L + U bands. Meanwhile, the IL is less than 1 dB, and the fabrication time is within a few minutes. The operating bandwidth can be customized by adjusting the period of CHLFBG. Additionally, increasing the length of the CHLFBG can significantly improve the suppression efficiency, exceeding 99.99% (-40 dB). Moreover, the CHLFBG is insensitive to temperature, axial strain, and bending, making it stable and reliable in practical applications.

© 2025 Optica Publishing Group under the terms of the Optica Open Access Publishing Agreement

# 1. Introduction

Optical fiber filters have been widely utilized in the fields of communications, sensing, and laser technology due to their low insertion loss, compact size, flexibility, and immunity to electromagnetic interference. With the rapid development of these fields, broadening operational bandwidth has become a crucial issue for fiber filters. Among various types of fiber filters, fiber gratings stand out as one of the most extensively employed due to their superior wavelength selectivity and integration capabilities. These devices are categorized into fiber Bragg gratings (FBGs) and long-period fiber gratings (LPFGs) based on their periodic structures. As bandrejection filters, FBGs are primarily used for narrow-band (0.1 nm-1 nm) [1,2] and moderate-band (1 nm-50 nm) [3,4] filtering applications. In recent years, studies on tilted FBGs (TFBGs) [5,6] and chirped and tilted FBGs (CTFBGs) [7,8] have demonstrated the feasibility of achieving hundred-nanometer scale of filtering bandwidth using FBG-based designs. However, no further research on achieving broader filtering bandwidths has been reported. Compared to FBGs, LPFGs typically exhibit larger filtering bandwidths (20 nm-200 nm) [9-11]. Regarding ultra-broadband performance, Zhao et al. reported a mode converter based on a chirped LPFG fabricated in a two-mode fiber, achieving a bandwidth of 405.3 nm [12]. Peng et al. demonstrated an LPFG-based mode converter in a tapered few-mode fiber, achieving a bandwidth of 504 nm [13]. Nevertheless, these filters involve complex fabrication processes and are incompatible with standard optical fiber systems. Moreover, due to the high environmental sensitivity of LPFGs, the stability of these filters remains a challenge. Beyond fiber gratings, research on ultra-broadband fiber filters has primarily focused on structured fibers [14–18]. Matsui et

al. fabricated an ultra-broadband acousto-optic mode converter based on a hole-assisted fiber, achieving a bandwidth of 120 nm [14]. Jin et al. demonstrated an ultra-broadband acousto-optic tunable filter based on a cladding-etched single-mode fiber, with a bandwidth of 362 nm [15]. Additionally, numerous ultra-broadband single-polarization filters have been designed based on various photonic crystal fiber structures [16–18]. Despite the remarkable filtering capability over hundreds of nanometers exhibited by these structured fiber-based designs, they still face significant challenges in complex fabrication processes and difficulties in compatibility with conventional optical fiber systems. In recent years, highly localized fiber Bragg gratings (HLFBGs) have been increasingly applied in the field of sensing, particularly for refractive index measurement [19–21], due to their ability to excite comb-like transmission spectra of cladding modes spanning several hundred nanometers. These broadband loss spectral characteristics, combined with the inherent advantages of FBGs—such as straightforward fabrication, high stability, and compatibility with optical fibers—render HLFBGs highly promising for broadband optical filtering applications. However, the comb-like transmission spectra result in low slope efficiency, which limits their effectiveness in filtering applications.

In this paper, we propose and demonstrate an ultra-broadband fiber filter based on a chirped highly localized fiber Bragg grating (CHLFBG). By introducing chirp into the HLFBG, the coupling peaks of numerous cladding modes are broadened and overlapped, resulting in a novel ultra-broadband and smooth loss spectral characteristic for the device. The CHLFBGs are fabricated using a femtosecond laser point-by-point inscription technique combined with the position synchronized output (PSO) function, enabling a filtering efficiency exceeding 90% (-10 dB) across a bandwidth greater than 500 nm, and the entire fabrication process requires only 100 seconds. The filtering bandwidth can be tuned by precise adjustment of the CHLFBG's grating pitch, while extended grating length enables exceptional filtering efficiency exceeding 99.99% (-40 dB attenuation).

# 2. Experimental principle and setup

#### 2.1. Principle of CHLFBGs

Firstly, the theoretical aspects of CHLFBG need to be introduced. For an HLFBG, all cladding modes  $EH_{lm}/HE_{lm}$  that can couple with the core mode  $HE_{11}$  have resonance wavelengths given by [22]:

$$\lambda = \frac{(\bar{n}_{11}(\lambda) + \bar{n}_{lm}(\lambda))\Lambda}{\nu} \tag{1}$$

where  $\bar{n}_{11}$  and  $\bar{n}_{lm}$  are the effective refractive indices of the HE<sub>11</sub> and EH<sub>lm</sub>/HE<sub>lm</sub> modes, respectively,  $\Lambda$  and  $\nu$  are the period and order of the grating, respectively. The resonance intensity of a given cladding mode depends on its coupling coefficient [22]:

$$\kappa_{lm} = \frac{2\pi c}{4\lambda} \cdot \int_{0}^{2\pi} d\Phi \int_{0}^{a_{1}} dr r \Delta \varepsilon(x, y, z) \boldsymbol{E}_{11}^{T} \cdot \boldsymbol{E}_{lm}^{T*}$$
(2)

where c is the speed of light in vacuum,  $a_1$  is the core radius,  $\Delta \varepsilon(\mathbf{x}, \mathbf{y}, \mathbf{z})$  is the perturbation of the dielectric constant,  $E_{11}^T$  and  $E_{1m}^{T*}$  are the transverse electric fields of the  $HE_{11}$  and  $EH_{im}/HE_{im}$  modes, respectively. Furthermore, if the grating period  $\Lambda$  increases linearly, then based on Eq. (1), the resonance wavelength of each cladding mode will be broadened as [7]:

$$\Delta \lambda \approx \frac{(\bar{n}_{11}(\lambda) + \bar{n}_{lm}(\lambda))(\Lambda_{max} - \Lambda_{min}))}{\nu}$$
(3)

where  $\Lambda_{\text{max}}$  and  $\Lambda_{\text{min}}$  are the maximum and minimum periods within a grating. According to Eq. (3), if the HLFBG is chirped, the resonance of each coupled cladding mode will experience a

certain degree of broadening, ultimately leading to significant overlap. Finally, over a broadband transmission spectrum, the originally dense comb-like profile will be replaced by a smoother and more continuous spectral profile. And as a filter, this optimized spectral profile is expected to demonstrate exceptional ultra-broadband suppression performance.

## 2.2. Experimental setup for fabricating CHLFBGs

As shown in Fig. 1(a), the CHLFBGs were fabricated by using a femtosecond laser (KY-Vibre, keyun) with a pulse duration of 195 fs, a central wavelength of 515 nm, and a repetition rate of 1 MHz in an SMF (G652D, YOFC) through a 100x oil-immersion objective (NA = 1.25). The SMF was fixed on an assembled 3D high-precision air-bearing translation stage (QFL100-100XY and RBN150V-5, AUS-PRECISION) which can move the fiber towards x, y and z-axis. Here, the implementation of chirping was based on the position synchronized output (PSO) function. Firstly, the initial pitch of the grating was determined according to the designed operating wavelength. Subsequently, a small incremental value was introduced, resulting in a linear increase in pitch size between successive grating periods. Then, the complete set of pitch values was stored as an array and imported into the controller of the 3D translation stage. Finally, the 3D translation stage moved along the x-axis according to the predefined distances in the array, while the controller simultaneously sent a high-level trigger signal to the laser at each designated position, generating a laser pulse and thereby completing the fabrication of the CHLFBG. Note that both the operating wavelength and chirp rate of the CHLFBG can be flexibly adjusted by modifying the first value and the incremental value in the array. The above process is also

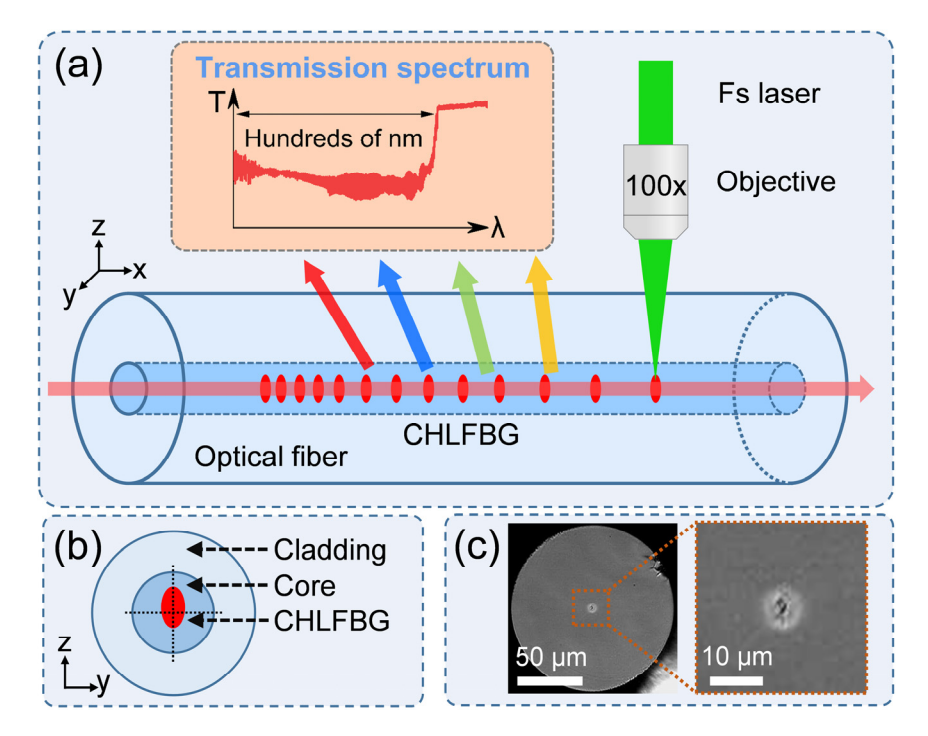


**Fig. 1.** (a) Schematic diagram for fabricating CHLFBG in SMF using femtosecond laser point-by-point technology, the inset demonstrates a typical transmission spectrum of CHLFBG; (b) schematic diagram of CHLFBG modulation position in the cross section of fiber; (c) cross-sectional microscopic image of CHLFBG and the enlarged image near the core region.

applicable to the fabrication of normal chirped fiber Bragg gratings (CFBGs). As shown in Fig. 1(b), the CHLFBG is asymmetrically positioned relative to the core in the cross-section of fiber. This asymmetrical modulation facilitates the excitation of a large number of cladding modes [23]. As shown in Fig. 1(c), the left image presents a microscopic cross-sectional view of the CHLFBG, while the right image is a magnified view focusing on the core region of the left image.

#### 3. Fabrication results and discussion

#### 3.1. Spectral differences between uniform HLFBG and chirped HLFBG

The spectral differences between uniform highly localized fiber Bragg grating (UHLFBG) and CHLFBG were then experimentally verified. In the experiment, a laser pulse energy of 70 nJ and a processing speed of 0.1 mm/s were set. The initial pitch was set to 0.580 µm, corresponding to a first-order grating with a Bragg wavelength of ~1680 nm. UHLFBG and CHLFBG were sequentially fabricated, of which lengths were 10 mm. And the CHLFBG had a chirp rate of 10 nm/cm. Unless otherwise specified, the following experiments were all conducted using the same fabrication parameters. A supercontinuum light source (SC-5, YSL Photonics) was used to offer the input light, and the spectrum was measured using a broadband optical spectrum analyzer (OSA, AQ6370D, YOKOGAWA) while the gratings were freely placed in the air. Since the detected signal was too weak below 1100 nm due to the high loss of the G652D fiber as well as the limited power of the light source, and the OSA operates up to 1700nm, the measurement range was set to 1100–1700nm.

As shown in Fig. 2(a), due to the resonance coupling between the core mode and all cladding modes that satisfy the phase matching condition, the transmission spectrum of the UHLFBG exhibits a densely packed broadband comb-like profile [23]. The resonance wavelength correlates with the effective refractive index (ERI) of the cladding mode, with shorter wavelengths corresponding to smaller ERIs. The cutoff mode, where the ERI matches the external medium, appears at 1425 nm, followed by the low-order cladding mode coupling peak at 1620 nm and the core mode coupling peak at 1680 nm, with coupling depths exceeding -40 dB, -40 dB, and -30 dB, respectively. Below the cutoff mode, leaky mode coupling is observed. Different to UHLFBG, introducing chirp in CHLFBG leads to a broadening of all cladding mode coupling peaks, resulting in significant overlap and ultimately forming a relatively continuous and smooth transmission spectrum. Acting as a filter, the CHLFBG provides optical rejection over a broad spectral range of 1100 nm to 1680 nm, covering more than 500 nm and encompassing the entire optical fiber communication bands (O + E + S + C + L + U). It achieves an average filtering efficiency of larger than -10 dB (90%), and an insertion loss of <1 dB in the long-wavelength region (>1680 nm). Figure 2(b) presents the reflection spectra of both gratings near the Bragg wavelength. Due to the introduction of chirp, the CHLFBG exhibits a broadened reflection spectrum compared to the UHLFBG, with a 3dB-bandwidth of ~10 nm. Figure 2(c) shows the top and side microscopic views of the CHLFBG. Note that at a processing speed of 0.1 mm/s, fabricating such a filter requires only 100 seconds, demonstrating a significant advantage in fabrication efficiency.

## 3.2. Studies on different fabrication parameters of CHLFBG

The spectral influence of different chirp rates on CHLFBG was investigated. As shown in Fig. 3(a), as the chirp rate increased from 2 nm/cm to 5 nm/cm, 10 nm/cm, and 20 nm/cm, the broadening of the cladding mode coupling peaks became increasingly pronounced. Consequently, the transmission spectrum became progressively smoother and more continuous. Meanwhile, it is observed that increasing the chirp rate does not significantly affect the filtering efficiency. Figure 3(b) compares the transmission spectra of these CHLFBGs from the cutoff mode

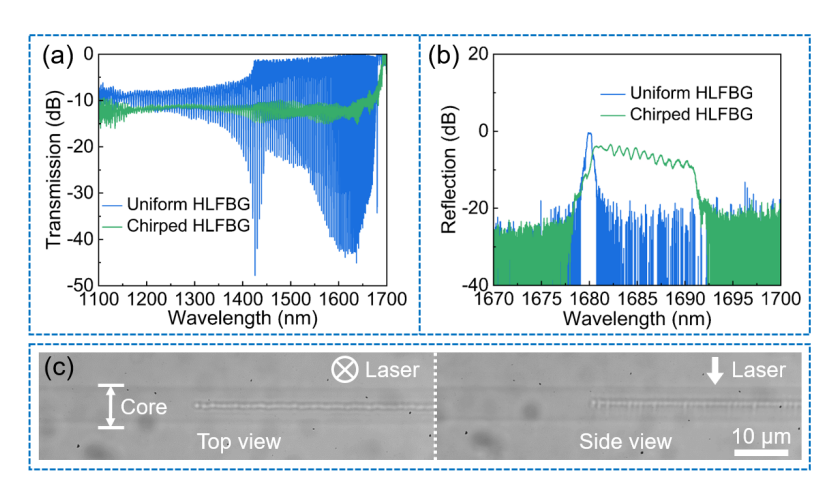


**Fig. 2.** (a) Transmission and (b) reflection spectra of uniform HLFBG and chirped HLFBG; (c) Top-view and side-view microscopic images of chirped HLFBG.

wavelength to the Bragg wavelength region, clearly illustrating the smoothing effect of the increasing chirp rate on the filter spectrum. When the chirp rate reached 20 nm/cm, the comb-like spectral profile became nearly unobservable. As shown in Fig. 3(c), with the chirp rate gradually increasing from 2 nm/cm to 20 nm/cm, the reflection bandwidth of the CHLFBG expanded proportionally. This further demonstrates the highly customizable reflection bandwidth control enabled by the PSO-based CFBG inscription technique.

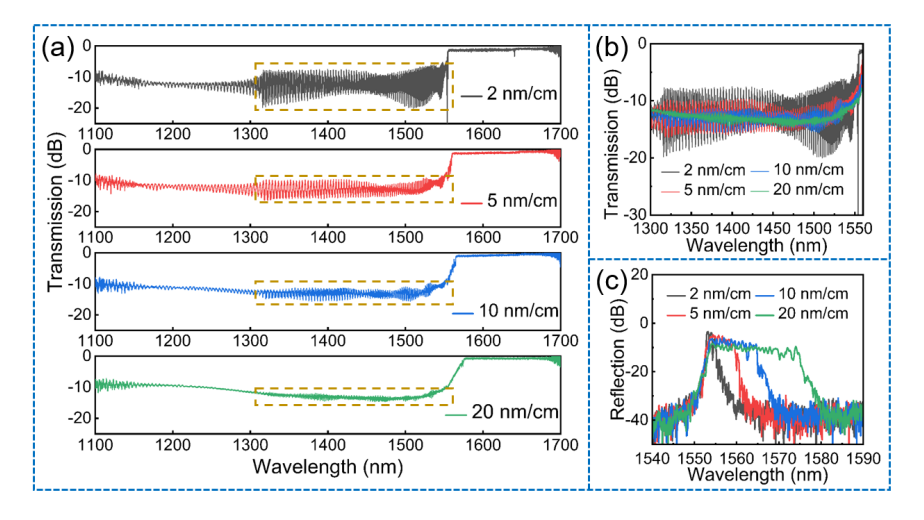


**Fig. 3.** Spectral differences of CHLFBGs with different chirp rates. (a) Broadband transmission spectra; (b) comb-like spectra in a localized wavelength range; (c) reflection spectra.

The femtosecond laser point-by-point inscription technique we used enables flexible grating pitch control, providing excellent wavelength-specific transmission characteristics and spectral bandwidth adjustability for optical filters. As shown in Fig. 4, when the initial pitch of the CHLFBG was set to  $0.414\,\mu m$ ,  $0.483\,\mu m$ ,  $0.552\,\mu m$ , and  $0.621\,\mu m$  (corresponding to first-order FBGs with Bragg wavelengths of  $1200\,n m$ ,  $1400\,n m$ ,  $1600\,n m$ , and  $1800\,n m$ , respectively), the filter's bandwidth increased from  $100\,n m$  to  $300\,n m$ ,  $500\,n m$ , and  $600\,n m$ . Meanwhile, the

average insertion loss remained below 1 dB, which enables the filter to be precisely tailored so that light with wavelengths shorter than a designated threshold is predominantly attenuated, while longer-wavelength light is largely preserved. Here, the average insertion loss of the CHLFBG is defined as the average loss on the long-wavelength side beyond the right cut-off wavelength (i.e., the designed threshold wavelength) of its filtering band. It should be noted that at the same length, CHLFBGs with shorter wavelengths have smaller pitches and thus contain more grating periods, leading to higher filtering efficiency and increased insertion loss, as illustrated in Fig. 4. Due to instrumental limitation, wider bandwidths are not further demonstrated here. However, it can be reasonably inferred that the operational bandwidth of this filter can fully cover the entire working waveband of the using fiber. Moreover, note that the filtering principle of the proposed CHLFBGs is applicable to various types of optical fibers. Therefore, this device also holds significant potential for fabrication and application in fibers operating at different wavelength ranges, which could extend its operational bandwidth to a broader spectral region.

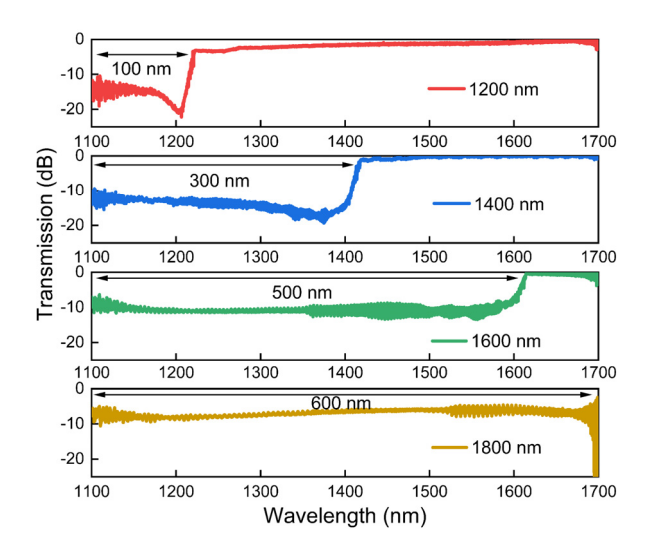


**Fig. 4.** Transmission spectra of CHLFBGs with different Bragg wavelengths.

To further enhance the filtering efficiency of this filter, the spectral impact of different lengths was investigated. Using an initial pitch of 0.535 µm, and a chirp rate of 20 nm/cm, CHLFBGs of varying lengths were fabricated. As shown in Fig. 5(a), when the length of CHLFBG increased from 5 mm to 10 mm, 20 mm, and 30 mm, the average filtering efficiencies within the operational bandwidth (1100 nm-1550 nm) reach -5.9 dB (74.3%), -11.5 dB (92.9%), -20.7 dB (99.1%), and an exceptionally high -40.2 dB (99.99%), respectively. Meanwhile, the average insertion losses were only 0.5 dB, 0.7 dB, 1.2 dB, and 2.2 dB, respectively. This experimental result demonstrated that the proposed filter exhibited an ultra-high filtering efficiency-to-insertion loss (FE-to-IL) ratio. It is also noted that as the length increased, the coupling loss of cladding modes beyond the cutoff mode wavelength increased significantly more than that in the shorter-wavelength region. Therefore, in future studies, it could be possible to achieve band-rejection filtering by reducing the fabricating pulse energy while simultaneously increasing the CHLFBG length. This approach would ensure that the loss in the short-wavelength region is minimized, effectively "closing" the short-wave side of the filter, while maximizing the coupling of cladding modes beyond the cutoff wavelength. Figure 5(b) illustrates the increasing trend of the FE-to-IL ratio with length. As the length increased from 5 mm to 30 mm, the FE-to-IL ratio of the CHLFBG gradually rose from 11.8 to 18.3.

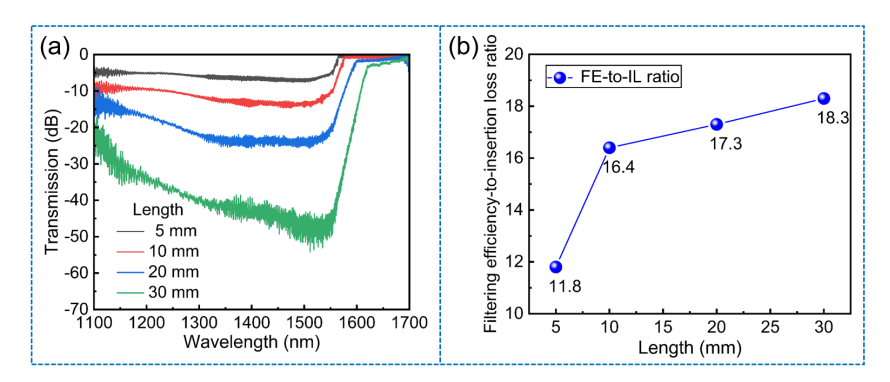


**Fig. 5.** (a) Transmission spectra and (b) filtering efficiency-to-insertion loss (FE-to-IL) ratio of CHLFBGs with different grating lengths.

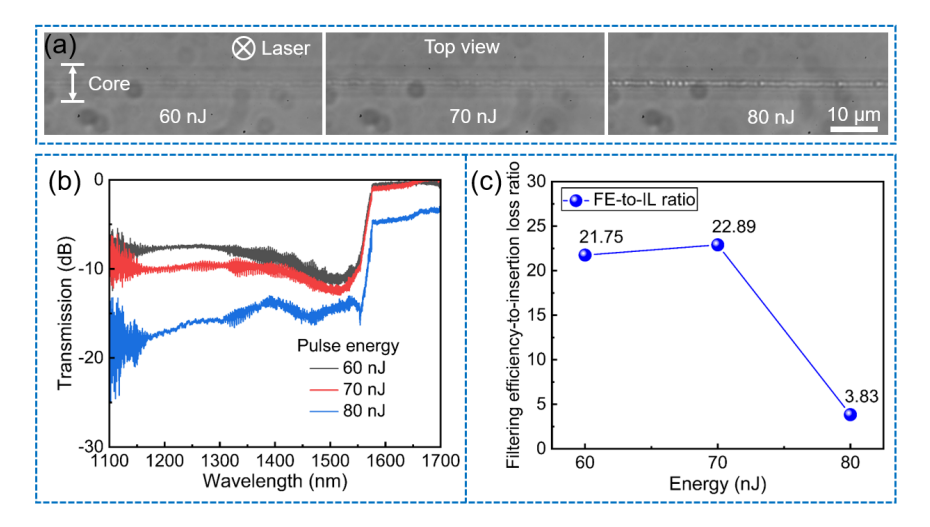


**Fig. 6.** (a) Top-view microscopic images, (b) transmission spectra and (c) filtering efficiency-to-insertion loss (FE-to-IL) ratios of CHLFBGs fabricated with different pulse energies.

In the experiment, the effect of different pulse energies on the CHLFBG spectrum was also investigated to optimize the selection of pulse energy. CHLFBGs were fabricated using pulse energies of 60 nJ, 70 nJ, and 80 nJ, all with a length of 10 mm, an initial pitch of 0.535 µm, and a chirp rate of 20 nm/cm. Figure 6(a) presents the top-view microscopic morphology of the CHLFBG under three different pulse energies. When the pulse energy was 60 nJ and 70 nJ, the laser modulation on the fiber core was relatively weak, and no obvious destructive structures were observed. However, when the pulse energy increased to 80 nJ, distinct black destructive structures appeared, and discontinuities began to emerge between periods. Consequently, excessively high pulse energy would significantly affect the performance of the CHLFBG. As shown in Fig. 6(b), the CHLFBG fabricated with 60 nJ exhibited an average filtering efficiency of -8.7 dB (86.5%) within the operational bandwidth (1100 nm-1550 nm), with an average insertion loss of 0.4 dB. When the pulse energy increased to 70 nJ, the average filtering efficiency improved to -10.3 dB (90.7%), while the average insertion loss slightly increased to 0.45 dB. However, when the pulse energy was further increased to 80 nJ, although the average filtering efficiency improved to -15.7 dB (97.3%), the average insertion loss increased disproportionately to 4.1 dB, leading to a substantial decline in the FE-to-IL ratio, which is unfavorable for practical applications.

Figure 6(c) clearly shows the FE-to-IL ratio under three different pulse energies, reaching a maximum value of 22.89 at 70 nJ. Therefore, the optimized pulse energy of 70 nJ was selected in the experiment, and an average insertion loss of <1 dB was adopted as the general criterion for fabricating CHLFBGs.

Additionally, we investigated the effect of different off-axis distances of the CHLFBG modulation position relative to the core center on its spectrum. CHLFBGs with varying off-axis distances were fabricated with an initial pitch of 0.535 µm, a chirp rate of 20 nm/cm, and a length of 10 mm. As shown in Fig. 7(a), the inset illustrates the cross-sectional positions of CHLFBGs with different off-axis distances. When the offset was 0 μm, 1 μm, and 2 μm, respectively, the coupling depth in the long-wavelength region within the operating bandwidth gradually decreased, while it slightly increased in the short-wavelength direction. This phenomenon occurred because, when the modulation position was at the core center, coupling primarily took place in cladding modes with a smaller azimuthal index l, corresponding to longer coupling wavelengths. However, as the modulation position gradually shifted away from the center, the coupling coefficients of cladding modes with larger l values increased, while those of modes with smaller l values decreased [23]. Moreover, with increasing off-axis distances, a slight decrease in average insertion loss was observed. Based on these results, for filtering applications, if a higher average filtering efficiency is desired, the CHLFBG should be inscribed at the fiber core center. Conversely, if spectrum flattening is preferred, an appropriate off-axis distance can be utilized. Figure 7(b) presents the top-view microscopic images of the CHLFBG under three different off-axis distances.

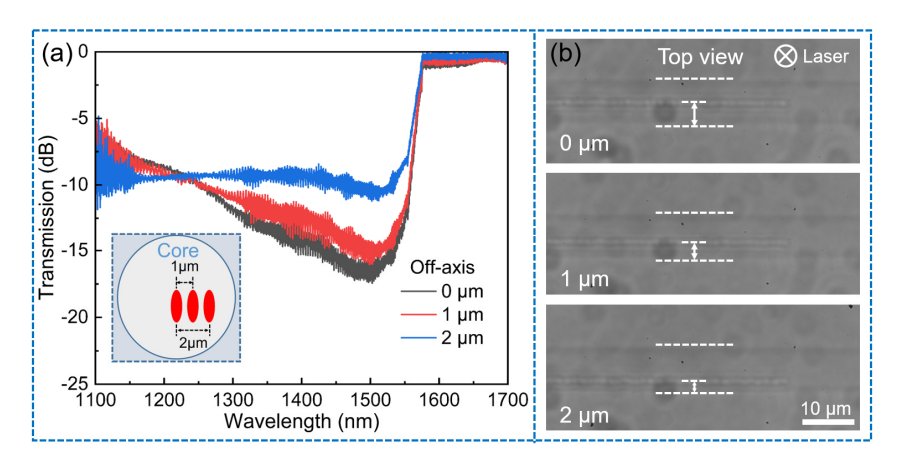


**Fig. 7.** (a) Transmission spectra and (b) top-view microscopic images of CHLFBGs with different off-axis distances. Inset: schematic in cross-sectional view of the CHLFBGs with different off-axis distances.

#### 4. Spectral stability tests of CHLFBG

The spectral stability of the CHLFBG was evaluated under different conditions, including varying temperature, axial strain, and bending. Each test was conducted three times for reproducibility. The tested CHLFBG had a length of 10 mm and a chirp rate of 20 nm/cm. Firstly, the temperature response of the CHLFBG was measured. The CHLFBG was placed in a high-precision column oven (LCO 102) with an accuracy of 0.1°C, where the temperature was controlled from 30°C to 90°C, with a holding time of 10 minutes at each measurement point. As shown in Fig. 8(a), when the temperature increased by 60°C, the average wavelength shift of the CHLFBG was only 0.69 nm, with a slope of 11.8 pm/°C. The right image presents the spectral variations observed in one of the temperature tests. Subsequently, axial strain testing was performed. One end of the CHLFBG was fixed to a stationary platform, while the other end was secured to a

one-dimensional manual translation stage with a resolution of  $10\,\mu m$ , with an initial separation of  $10\,cm$  between the two ends. The translation stage was moved  $40\,\mu m$  per step, inducing an axial strain of  $400\,\mu \epsilon$  in the CHLFBG, and the spectral response was measured for strain values ranging from 0 to  $2000\,\mu \epsilon$ . As shown in Fig. 8(b), when the axial strain increased from 0 to  $2000\,\mu \epsilon$ , the average wavelength shift was only  $1.20\,n m$ , with a slope of  $0.6\,p m/\mu \epsilon$ . The right image illustrates the spectral variations observed in one of the axial strain tests. Additionally, bending tests were conducted by placing the CHLFBG onto a customized curvature plate with different bending radii. As shown in Fig. 8(c), when the bending radius was reduced from 15 cm to  $2.5\,c m$ , the maximum variation in the average dip (within the  $1100-1550\,n m$  wavelength range) was only  $0.44\,d B$ . The right image shows the spectral variations observed in one of the

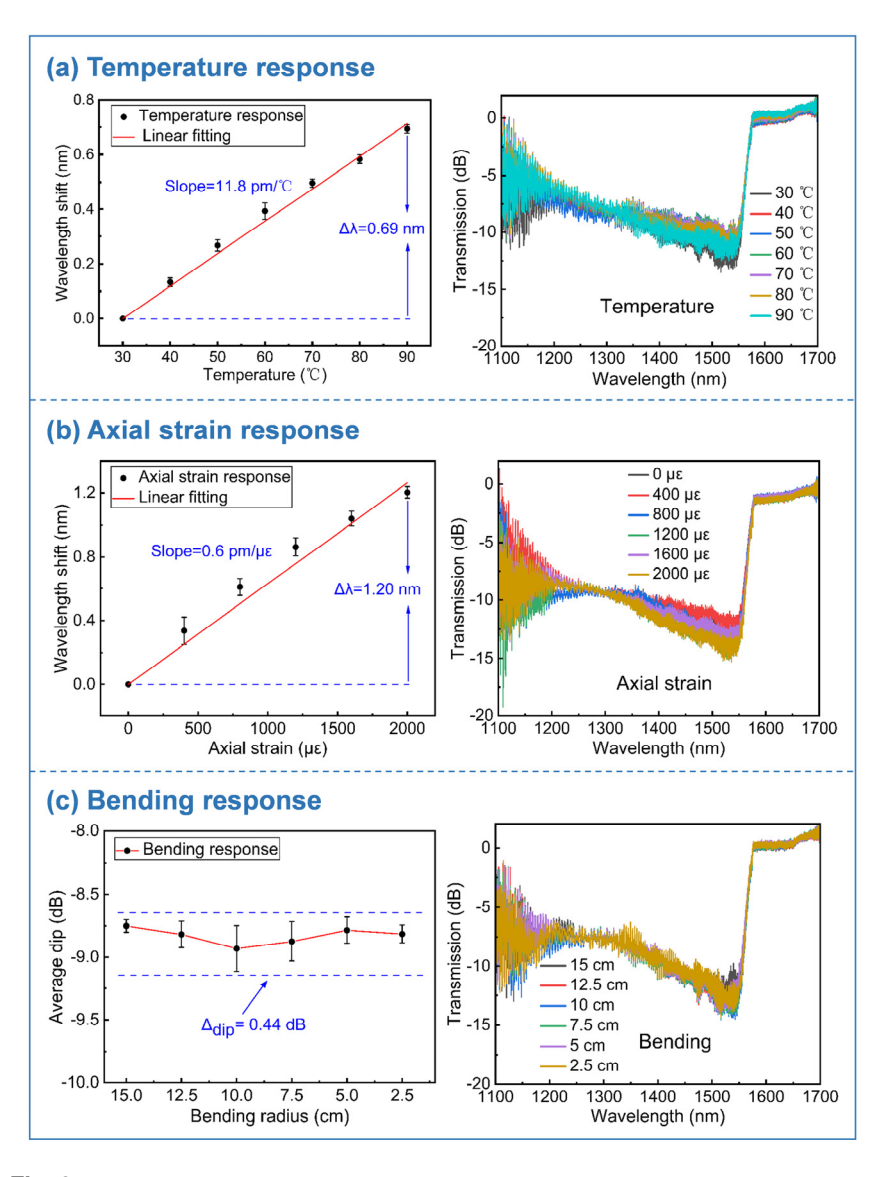


**Fig. 8.** Spectral stability tests of the obtained CHLFBG. (a) Temperature response from  $30^{\circ}\text{C}$  to  $90^{\circ}\text{C}$ . (b) Axial strain response from 0 to  $2000~\mu\epsilon$ . (c) Bending response: bending radius from 15~cm to 2.5~cm.

bending tests. These experimental results demonstrate that the fabricated CHLFBG exhibits high insensitivity to temperature, axial strain, and bending. Compared to other grating-based broadband filters, particularly those based on LPFGs and structured fibers, the CHLFBG offers significant advantages in stability and robustness.

#### 5. Conclusion

In conclusion, we have proposed and experimentally demonstrated an ultra-broadband fiber filter utilizing a CHLFBG, fabricated through femtosecond laser point-by-point technology combined with the PSO function. The highly localized inscription of core-asymmetric gratings in a standard single-mode fiber (SMF) achieved efficient excitation of multiple cladding modes. Furthermore, these cladding modes were broadened and overlapped, and consequently formed a filter with a bandwidth over 500 nm and an average filtering efficiency over 90% (-10 dB). The experimental results demonstrated that the bandwidth of CHLFBG could be flexibly customized by adjusting the initial pitch. Additionally, increasing the chirp rate significantly suppressed the original comb-like transmission spectrum of the HLFBG, generating a smoother and more continuous spectral profile. Length-dependent optimization of CHLFBGs achieved exceptional filtering efficiency exceeding 99.99% (-40 dB attenuation), while maintaining minimal insertion loss escalation ( $\Delta$ IL = 2.2 dB). The impact of different fabrication pulse energies and off-core positions on the CHLFBG spectrum were also investigated. Moreover, the experimental results indicated that the CHLFBG was insensitive to temperature, axial strain, and bending, enabling it great candidate for ultra-wide spectral filtering.

**Funding.** National Key Research and Development Program of China (2023YFB3209500); National Natural Science Foundation of China (U22A2088); Shenzhen Science and Technology Program (JCYJ20241202124226032); Shenzhen Key Laboratory of Ultrafast Laser Micro/Nano Manufacturing (ZDSYS20220606100405013).

**Disclosures.** The authors declare no conflicts of interest.

**Data availability.** Data underlying the results presented in this paper are not publicly available at this time but may be obtained from the authors upon reasonable request.

#### References

- J. Canning, D. C. Psaila, Z. Brodzeli, et al., "Characterization of apodized fiber Bragg gratings for rejection filter applications," Appl. Opt. 36(36), 9378–9382 (1997).
- J. K. Sahota, N. Gupta, and D. Dhawan, "Fiber Bragg grating sensors for monitoring of physical parameters: a comprehensive review," Opt. Eng. 59(06), 1 (2020).
- 3. X. Dong, P. Shum, X. Yang, *et al.*, "Bandwidth-tunable filter and spacing-tunable comb filter with chirped-fiber Bragg gratings," Opt. Commun. **259**(2), 645–648 (2006).
- D. Tosi, "Review of chirped fiber Bragg grating (CFBG) fiber-optic sensors and their applications," Sensors 18(7), 2147 (2018).
- J. Albert, L. Y. Shao, and C. Caucheteur, "Tilted fiber Bragg grating sensors," Laser & Photonics Reviews 7(1), 83–108 (2013).
- T. Guo, F. Liu, B. O. Guan, et al., "Tilted fiber grating mechanical and biochemical sensors," Opt. Laser Technol. 78, 19–33 (2016).
- F. Liu, T. Guo, C. Wu, et al., "Wideband-adjustable reflection-suppressed rejection filters using chirped and tilted fiber gratings," Opt. Express 22(20), 24430–24438 (2014).
- T. X. Duan, X. Y. Li, R. H. Wang, et al., "Femtosecond laser plane-by-plane inscription of chirped and tilted fiber Bragg gratings," J. Lightwave Technol. 42(17), 6083–6089 (2024).
- 9. A. M. Vengsarkar, P. J. Lemaire, J. B. Judkins, *et al.*, "Long-period fiber gratings as band-rejection filters," J. Lightwave Technol. **14**(1), 58–65 (1996).
- K. Chen, Q. Q. Sheng, and X. Y. Dong, "Band-rejection and bandpass filters based on mechanically induced long-period fiber gratings," Microw. Opt. Technol. Lett. 42(1), 15–17 (2004).
- 11. Y. P. Wang, "Review of long period fiber gratings written by CO2 laser," J. Appl. Phys. 108(8), 081101 (2010).
- X. Y. Zhao, Z. Y. Liu, F. Wang, et al., "Bandwidth Tunable Ultra-Broadband OAM Generators Based on Chirped Long Period Fiber Gratings at Dispersion Turning Point," J. Lightwave Technol. 42(14), 4980–4986 (2024).
- 13. W. Peng, Y. H. Ma, Y. Zhu, *et al.*, "Broadband wavelength-tunable mode converter based on long-period fiber gratings," J. Lightwave Technol. **36**(10), 649–652 (2024).

- 14. T. Matsui, K. Nakajima, K. Shiraki, *et al.*, "Ultra-broadband mode conversion with acousto-optic coupling in hole-assisted fiber," J. Lightwave Technol. **27**(13), 2183–2188 (2009).
- 15. T. Jin, Q. Li, J. H. Zhao, *et al.*, "Ultra-broad-band AOTF based on cladding etched single-mode fiber," IEEE Photonics Technol. Lett. **14**(8), 1133–1135 (2002).
- L. H. Jiang, Y. Zheng, J. Z. Yang, et al., "An Ultra-broadband single polarization filter based on plasmonic photonic crystal fiber with a liquid crystal core," Plasmonics 12(2), 411–417 (2017).
- L. H. Jiang, C. Wang, J. H. Zou, et al., "Design of two miniaturized and broadband polarization filters based on two types of square-lattice gold-filled photonic crystal fibers," Opt. Fiber Technol. 61, 102454 (2021).
- Y. C. Liu, H. L. Chen, S. G. Li, et al., "Surface plasmon resonance induced tunable ultra-wideband polarization filters based on gold film coated photonic crystal fibers," Opt. Laser Technol. 107, 174–179 (2018).
- 19. H. Chikh-Bled, M. Debbal, M. Chikh-Bled, *et al.*, "Refractive index sensor in eccentric fiber Bragg gratings using a point-by-point IR femtosecond laser," Appl. Opt. **58**(3), 528–534 (2019).
- K. M. Yang, B. N. Liu, C. R. Liao, et al., "Highly Localized Point-by-Point Fiber Bragg Grating for Multi-Parameter Measurement," J. Lightwave Technol. 39(20), 6686–6690 (2021).
- 21. J. He, R. X. Chen, X. Z. Xu, *et al.*, "Slit Beam Shaping for Femtosecond Laser Point-by-Point Inscription of Highly Localized Fiber Bragg Grating," J. Lightwave Technol. **40**(16), 5722–5728 (2022).
- J. U. Thomas, N. Jovanovic, R. G. Krämer, et al., "Cladding mode coupling in highly localized fiber Bragg gratings II: complete vectorial analysis," Opt. Express 20(19), 21434–21449 (2012).
- 23. J. U. Thomas, N. Jovanovic, R. G. Becker, *et al.*, "Cladding mode coupling in highly localized fiber Bragg gratings: modal properties and transmission spectra," Opt. Express **19**(1), 325–341 (2011).